Chaotic-to-regular transition in a semiclassical electron gas

S. D. Prado[1] and M. A. M. de Aguiar[2]

[1]*School of Mathematics, University of Bristol, Bristol BS8 1TW, United Kingdom*
[2]*Instituto de Física Gleb Wataghin, Universidade Estadual de Campinas, Campinas 13083-970, São Paulo, Brazil*

(Received 21 August 1995)

We study the magnetic susceptibility χ of a two-dimensional noninteracting electron gas confined by a smooth chaotic potential. The computation of χ for a wide range of magnetic field values B reveals that the chaotic ($B=0$) to regular ($B\rightarrow\infty$) transition is dominated by bifurcations of short periodic orbits that become stable as B increases. The families of stable orbits and tori contained in the associated stability islands do not play any special role in this regime. Large contributions, however, are observed near the bifurcation points, increasing the average susceptibility to values beyond those expected for regular systems. [S1063-651X(96)03107-8]

PACS number(s): 05.45.+b, 05.30.Fk, 03.65.Sq

I. INTRODUCTION

The recent experiment of Lévy *et al.* [1] has renewed theoretical interest in the semiclassical behavior of a two-dimensional (2D) ballistic electron gas subjected to a perpendicular constant magnetic field [2–5]. Efforts in this direction have so far been concerned with the low-field and low-temperature regime. The magnetic properties of these ''mesoscopic'' systems depend both on the underlying classical motion and on the characteristic thermodynamical ensemble. In particular, it has been shown by Altshuler, Gefen, and Imry [6], that averaging the magnetic susceptibility χ over an ensemble of ''large'' systems gives $\langle\chi\rangle\simeq0$ if it is computed within the grand-canonical ensemble. In this case, each subsystem is assumed to have a particular (fixed) chemical potential. By contrast, averaging over the canonical ensemble (CE) (i.e., with the number of particles in each subsystem held fixed) produces a large mean as compared to the Landau susceptibility.

Based on these results, Ullmo, Richter, and Jalabert [5] derived analytical expressions for $\langle\chi\rangle$ under the conditions of the Lévy experiment, in which the electrons were confined in a square billiard and subjected to a very weak magnetic field. They then showed that the shortest family of periodic orbits with a nonzero enclosed area gives the main contribution to the high values attained by χ. In other words, the one-parameter families of closed orbits existing in integrable systems interfere constructively and give a total contribution much larger than that of the isolated periodic orbits typical of chaotic confining potentials.

In this paper we study the susceptibility χ for a system subjected to a uniform magnetic field B. We compute $\chi(B)$ numerically at zero temperature for a wide range of magnetic fields, with the classical dynamics varying from regular to chaotic. For low fields, our results agree with the previous theory, in that the regular case displays a larger χ. As the field increases, however, several short periodic orbits become stable through isochronous (same period) and period-doubling bifurcations, giving rise to semiclassically divergent contributions to χ at the bifurcation points. Quantum mechanically these divergences are replaced by large but finite peaks. It turns out that these dominate the behavior of

χ for a large range of magnetic fields and make its average larger than in an equivalent regular situation. After the bifurcations, each newly stable orbit carries with it a stability island containing, to first approximation, a one-parameter family of closed orbits. Interestingly, our numerical results show that the contributions of these families are not relevant here, unlike in the zero field limit.

This paper is organized as follows: in Sec. II we review the semiclassical theory of a 2D noninteracting electron gas. In Sec. III we present our model for the numerical calculations, then, in Sec. IV, we show the results for $T=0$. Section V is devoted to our conclusions.

II. REVIEW OF THE SEMICLASSICAL THEORY

The exact expressions for the magnetization M and susceptibility χ in the canonical ensemble (CE) can be derived from the grand-canonical potential [6]

$$\Omega=-\frac{1}{\beta}\int dE\rho(E)\ln(1+e^{\beta(\mu-E)}), \tag{1}$$

where ρ is the density of states, $\beta=1/k_BT$, and μ is the chemical potential or Fermi level. Quantum mechanically, $\rho(E)=\Sigma\,\delta(E-E_n)$ for bound systems and

$$\Omega=-\frac{1}{\beta}\sum_n\ln(1+e^{\beta(\mu-E_n)}). \tag{2}$$

Therefore, in the grand-canonical ensemble (GCE) we can write explicitly

$$M_{\text{GCE}}\equiv-\frac{\partial\Omega}{\partial B}=-\sum_n g_\beta(E_n)\frac{\partial E_n}{\partial B} \tag{3}$$

and

$$\chi_{\text{GCE}}\equiv-\frac{\partial^2\Omega}{\partial B^2}$$
$$=-\sum_n g_\beta(E_n)\frac{\partial^2 E_n}{\partial B^2}+\sum_n\delta_\beta(E_n-\mu)\left(\frac{\partial E_n}{\partial B}\right)^2, \tag{4}$$

54   1369

where

$$g_\beta(E_n) = \frac{1}{1 + e^{\beta(E_n - \mu)}} \qquad (5)$$

is the Fermi function, and

$$\delta_\beta(E_n - \mu) \equiv \frac{\beta}{4\cosh^2\frac{\beta}{2}(E_n - \mu)} \qquad (6)$$

is a smoothed δ function.

The first term on the right side of Eq. (4) contains the contributions from the energy level curvatures, while the second term is responsible for dips in $-\chi_{\text{GCE}}$ whenever an energy level crosses the (fixed) value μ. These dips tend to disappear as the temperature is increased.

In the canonical ensemble we use the relation (see [6])

$$M_{\text{CE}} \equiv -\left(\frac{\partial F}{\partial B}\right)_P = -\left(\frac{\partial\Omega}{\partial B}\right)_{\mu = \frac{\partial F}{\partial N}\big|_B}, \qquad (7)$$

where F is the free energy and P is the number of particles, now held fixed. Therefore,

$$M_{\text{CE}} = -\sum_n g_\beta(E_n)\frac{\partial E_n}{\partial B}, \qquad (8)$$

where $g_\beta(E_n)$ is computed with $\mu = \mu(B)$ obtained from the constraint

$$P = \sum_{n=1}^\infty g_\beta(E_n(B)) = \sum_{n=1}^\infty \frac{1}{1 + e^{\beta(E_n(B) - \mu)}}. \qquad (9)$$

Differentiating Eq. (8) with respect to B gives

$$\chi_{\text{CE}} = -\sum_n g_\beta(E_n)\frac{\partial^2 E_n}{\partial B^2} + \sum_n \delta_\beta(E_n - \mu)$$
$$\times\left[\left(\frac{\partial E_n}{\partial B}\right)^2 - \left(\frac{\partial E_n}{\partial B}\right)\left(\frac{\partial\mu}{\partial B}\right)\right]. \qquad (10)$$

At low temperatures the Fermi level $\mu(B)$ is approximately the Pth energy level, $\mu(B) \approx E_P(B)$, and the second term on the right side does not contribute. In this limit, if the energy levels exhibit narrowly avoided crossings $-\chi_{\text{CE}}$ will also exhibit dips due to the sharpness of $\partial^2 E_P/\partial B^2$. Again, even very small temperatures will cause these to disappear.

Semiclassical expressions for M and χ are easily obtained with the help of Gutzwiller's formula for the density of states [7]. Rewriting the magnetization as (see [2])

$$M = \int_0^\infty g_\beta(E)\frac{\partial N}{\partial B}dE, \qquad (11)$$

where

$$N(E,B) = \sum_n \Theta(E - E_n(B)) \qquad (12)$$

is the staircase function, and using the semiclassical formula

$$N(E,B) \approx \bar{N}(E,B) + N^{osc}(E,B) \qquad (13)$$

we get, in the limit of low temperatures and for a 2D system,

$$M \approx \bar{M}(B) + \frac{2}{\beta\hbar}\sum_p\sum_j\frac{A_{p,j}a_p}{j\tau_p}\sin\left(\frac{jS_p}{\hbar} - \frac{\pi}{2}j\tau_p\right)$$
$$\times\frac{e^{-\pi\tau_p j/\hbar\beta}}{1 - e^{-2\pi\tau_p j/\hbar\beta}}. \qquad (14)$$

Here $\bar{M}$ comes from the corrections to the Weyl formula for $\bar{N}$,

$$\bar{N} = \frac{1}{\hbar^2}\int\Theta(E - H(p,q))d^2p\,d^2q + O(\hbar^0) \qquad (15)$$

and is usually very small. The second term in Eq. (14) is a sum over primitive periodic orbits, (p) and their repetitions (j), S_p, σ_p, τ_p being the action, Maslov index and period of the primitive orbits, respectively. The amplitude involves both

$$A_{pj}^{-1} = \sqrt{|\det(M_p^j - 1)|}$$
$$= \begin{cases} 2\sinh(ju/2) & \text{for direct unstable orbits} \\ 2\sin(ju/2) & \text{for stable orbits} \\ 2\cosh(ju/2) & \text{for inverse unstable orbits} \end{cases} \qquad (16)$$

where M_p is the Monodromy matrix, and $a_p = \partial S/\partial B$. All quantities in Eq. (14) are evaluated at the Fermi energy $\mu = \mu(B)$ in the canonical ensemble or at $\mu = \mu_0$ in the grand-canonical ensemble.

Differentiating Eq. (14) with respect to B, neglecting terms of $O(\hbar^{-1})$, then gives

$$\chi \approx \chi^L + \frac{2}{\beta\hbar^2}\sum_p\sum_j\frac{A_{p,j}a_p^2}{j\tau_p}\cos\left(\frac{jS_p}{\hbar} - \frac{\pi}{2}j\sigma_p\right)\frac{e^{-\pi\tau_p j/\hbar\beta}}{1 - e^{-2\pi\tau_p j/\hbar\beta}} \qquad (17)$$

where $\chi^L = \partial\bar{M}/\partial B$ is the Landau susceptibility.

In 2D integrable systems the periodic orbits come in one-parameter families (tori) on the energy shell, whereas in chaotic systems the orbits are isolated. It was shown in Ref. [5] that nearly integrable systems have an enhanced susceptibility due to the existence of these families. This is a consequence of the fact that the amplitude of the oscillatory part of the level density is proportional to $1/\hbar^{3/2}$ for integrable systems and only to $1/\hbar$ for chaotic systems.

The effect we are interested in concerns the transition, as the magnetic field increases, from a chaotic to a more regular phase space. This transition occurs generically through two basic mechanisms: the first is the isochronous bifurcation, in which a pair of periodic orbits, one stable and the other unstable, appears suddenly; this is also called a saddle-center bifurcation. The second possibility is an inverse period-doubling bifurcation, in which an unstable orbit becomes stable generating a new unstable orbit with twice the original period. If the Hamiltonian has at least one discrete symmetry, the isochronous bifurcation can also occur via the pitchfork (or inverse pitchfork) mechanism, if the periodic orbit is symmetric [8,9]. Then, a pair of new asymmetric orbits (one

TABLE I. Fermi energy at $B=0$ for the relevant values of P and $\hbar$.

$P\backslash\hbar$	0.006	0.06
30	0.0308	0.3146
50	0.0401	0.4030
120	0.0620	-

being the reflection of the other) is generated. In both cases, isochronous and period doubling, as the magnetic field is increased further the newly born unstable orbits become stable via subsequent period-doubling bifurcations. The stable orbits in turn then undergo higher order bifurcations whenever the stability angle u passes through $2\pi k/m$ (k, m coprime, $k<m$). Ozorio de Almeida and Hannay [10] have computed the amplitudes A_{pj} for these so-called resonant cases. At the saddle-center bifurcation, for instance, $A_{p1}\simeq 1/\hbar^{1/6}$. The higher order bifurcations with $m>4$, on the

other hand, contribute a factor $A_{p1}\simeq 1/\hbar^{1/2}$ which, as remarked in Ref. [10], is of the same magnitude as the resonant periodic orbit contribution in integrable systems obtained by Richens [11]. This means that in the transition regime between chaos and regularity, the susceptibility may be of the same semiclassical order as in the integrable case, and hence much larger than the small magnitudes expected at $B=0$. A numerical example showing this regular-to-chaotic transition and the role of bifurcations in the susceptibility will be presented in the next two sections.

III. THE MODEL AND ITS PROPERTIES

In this section we investigate the zero temperature magnetic properties of the same model system considered in Ref. [2], namely,

$$H=\frac{1}{2}\left(p_x+\frac{B}{2}y\right)^2+\frac{1}{2}\left(p_y-\frac{B}{2}x\right)^2+\left(y-\frac{x^2}{2}\right)^2+0.05x^2.$$
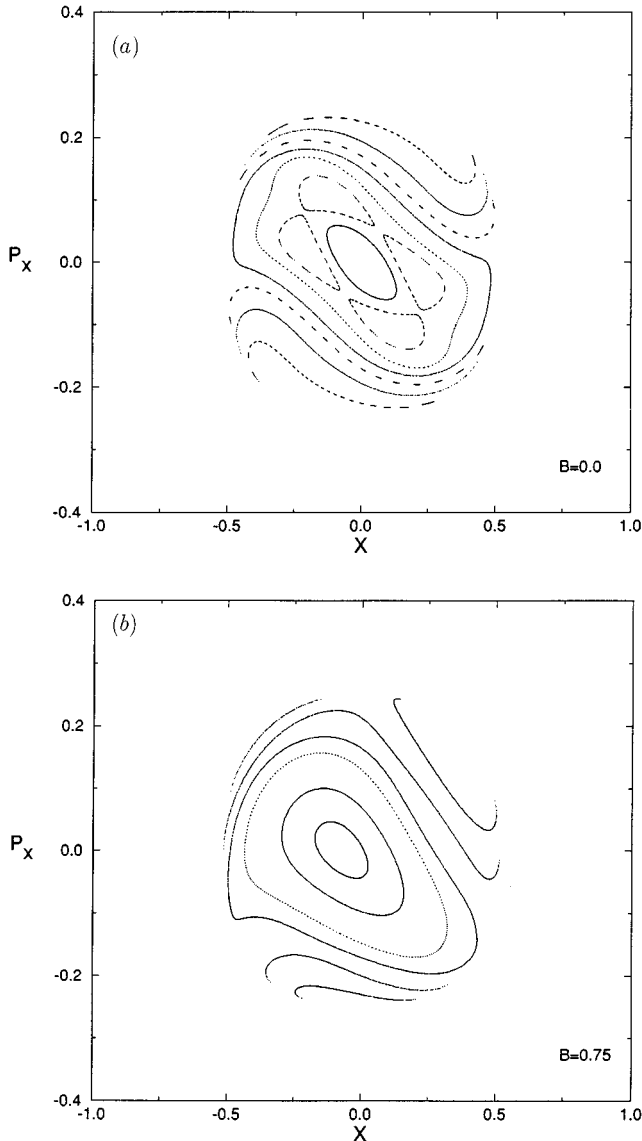$$(18)$$

FIG. 1. $x-p_x$ Poincaré sections at energy $E=0.0308$ ($\hbar=0.006$, $P=30$) and magnetic fields: (a) $B=0$; (b) $B=0.75$.

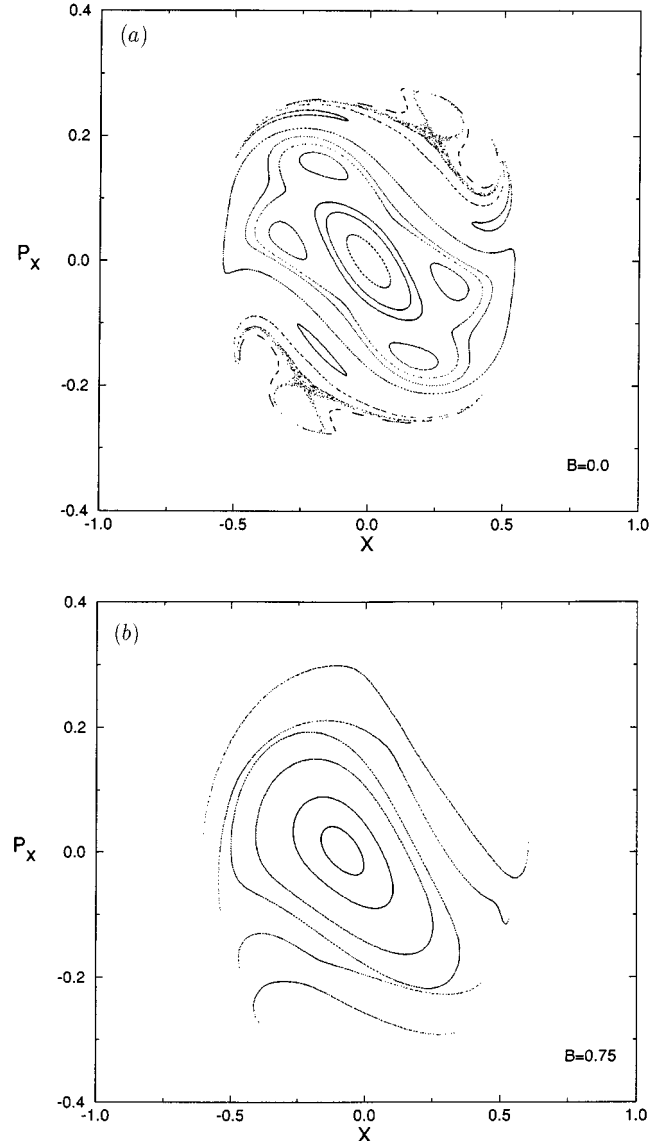FIG. 2. $x-p_x$ Poincaré sections at energy $E=0.0401$ ($\hbar=0.006$, $P=50$) and magnetic fields: (a) $B=0$; $B=0.75$.
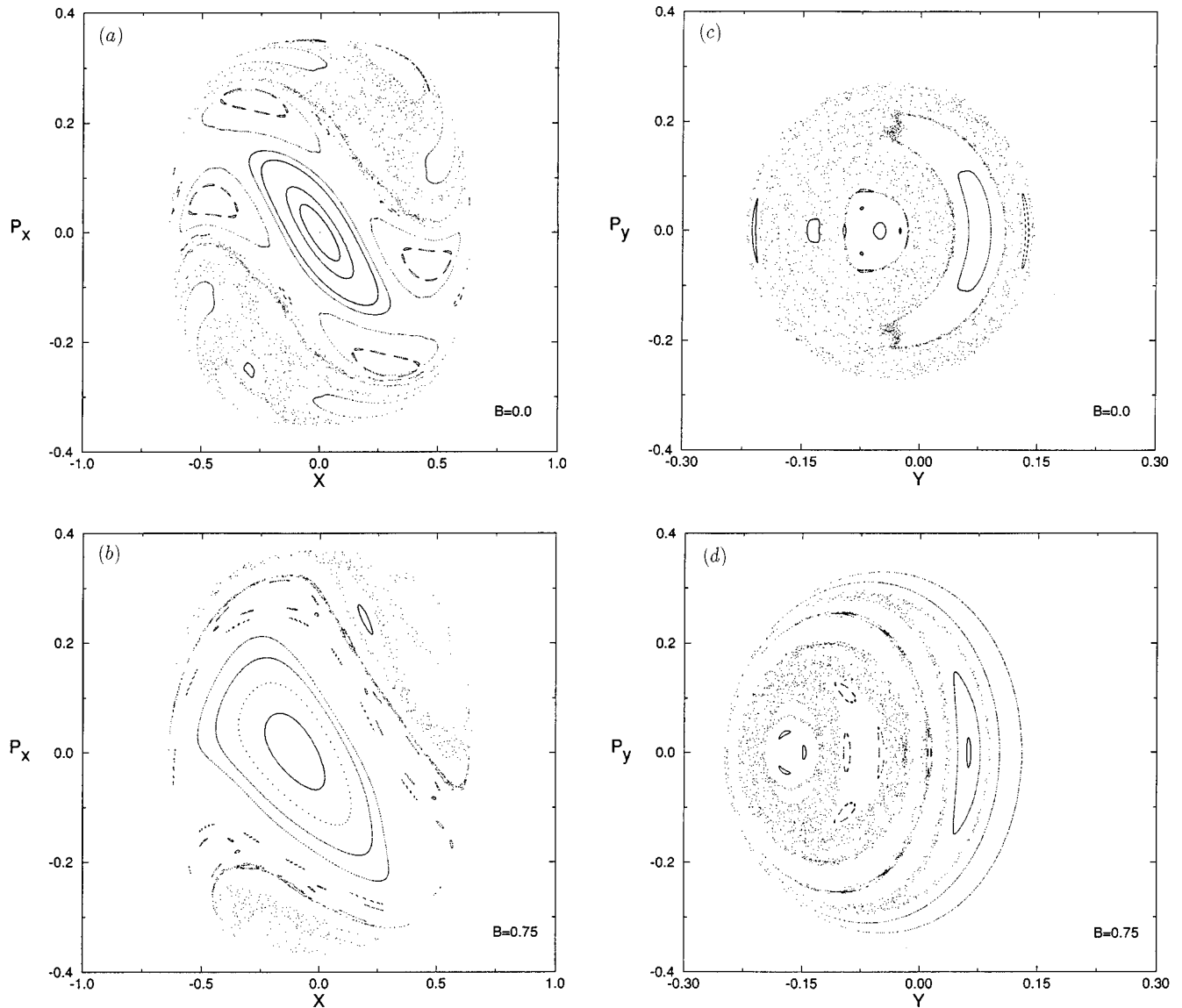
FIG. 3. Poincaré sections at energy $E = 0.062$ ($\hbar = 0.006$, $P = 120$): (a) and (b) show $x - p_x$ sections at $B = 0$ and $B = 0.75$; (c) and (d) show $y - p_y$ sections for the same values of B.

In order to compare regular versus chaotic features we have performed calculations with two values of $\hbar$. For $\hbar = 0.006$, the first 50 states have such small energies that the corresponding classical trajectories are effectively regular for any value of B. For $\hbar = 0.06$ the level spacing is larger and most of the eigenstates move into the classically chaotic region (of course, a few eigenstates—around seven in our case—have low energies and still lie in the regular region).

We have used two different basis states to diagonalize H, depending on the value of B. For $B < 0.6$ we used $\Phi_{nm}(x,y) = \langle n | x \rangle \langle m | y - x^2/2 \rangle$ where $|n\rangle$ and $|m\rangle$ are eigenstates of the harmonic part of H with $B = 0$ (see [12]). For $B \geq 0.6$ we used the exact solutions of $H^o = [p_x + (B/2)y]^2/2 + [p_y - (B/2)x]^2/2 + y^2 + 0.05x^2$ as basis states. For $\hbar = 0.006$ we obtained 120 eigenstates with at least five digits of precision for B in the range 0 to 1.5 in steps of $dB = 0.05$, while for $\hbar = 0.06$ only 70 eigenstates were considered.

The Weyl approximation for the staircase function is, in this case,

$$N_W(E) = \frac{E^2}{2\sqrt{0.2}\,\hbar^2}$$

and hence the energy of the nth level is proportional to $\hbar$. We must therefore scale the calculations for $\hbar = 0.006$ by a factor 10 before comparing them to those with $\hbar = 0.06$.

According to the semiclassical results of the preceding section, the behavior of χ is dictated by the classical orbits at the Fermi energy μ, which, in turn, depends on the number of particles P and on the magnetic field B via Eq. (9). It is therefore important to know whether the phase space at energy μ and magnetic field B is mostly regular, mixed, or mostly chaotic, in order to understand the magnitude and oscillations of χ. We emphasize that the few regular states of the *chaotic case* $\hbar = 0.06$ do not play an important role, since
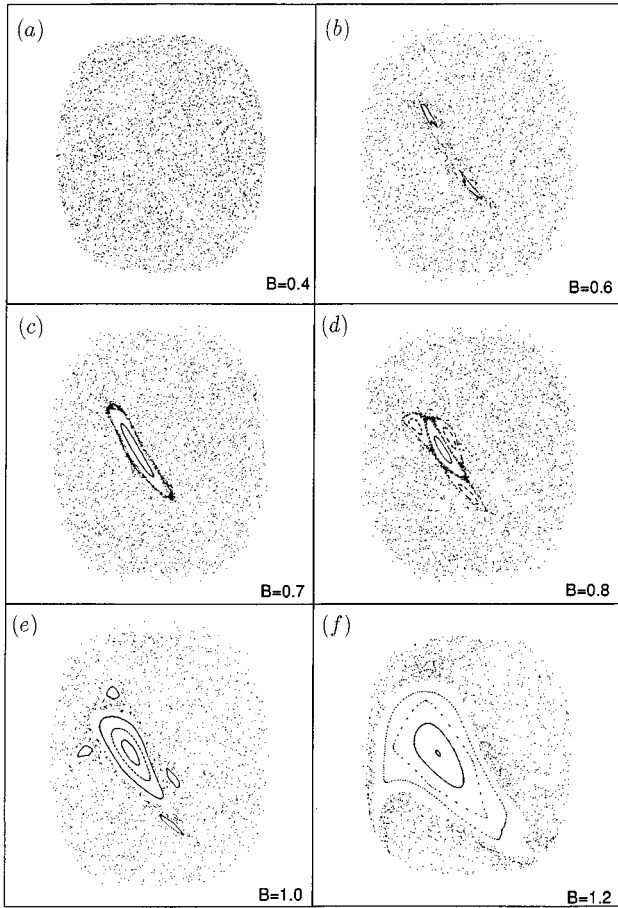
FIG. 4. $x - p_x$ Poincaré sections at energy $E = 0.3146$ ($\hbar = 0.06$, $P = 30$) and magnetic fields: (a) 0.4; (b) 0.6; (c) 0.7; (d) 0.8; (e) 1.0; (f) 1.2.

all classical quantities are calculated at $\mu(B) = E_P(B)$, which is a chaotic energy shell for $P \geqslant 10$.

In the next section we shall present results for the susceptibility with $P = 30$ and $P = 50$ for both values of $\hbar$, and for $P = 120$ when $\hbar = 0.006$. The Fermi energy in each case at $B = 0$ is given in Table I.

Figures 1 and 2 show the $x - p_x$ Poincaré sections at $B = 0$ and $B = 0.75$ for the energies 0.0308 ($P = 30$, $\hbar = 0.006$) and 0.0401 ($P = 50$, $\hbar = 0.006$), respectively. In all cases, the sections reveal a very regular phase-space structure which, in fact, extends to all values of B. Figure 3 shows $x - p_x$ and $y - p_y$ sections at $E = 0.0620$ ($P = 120$, $\hbar = 0.006$). In this case the dynamics are clearly mixed.

Figure 4 shows a detailed sequence of six $x - p_x$ Poincaré sections at $E = 0.3146$ ($P = 30$, $\hbar = 0.06$) for $B = 0.4$, 0.6, 0.7, 0.8, 1.0 and 1.2. As expected, the magnetic field tends to regularize the dynamics. In Fig. 5, the $x - p_x$ sections at $E = 0.4030$ ($P = 50$, $\hbar = 0.06$) for $B = 0.5$ and $B = 1.0$ show basically the same behavior.

Although the Poincaré sections allow a qualitative view of the global behavior of the system, it is difficult to specify the field value where any given periodic family bifurcates. Of particular importance in our study is the behavior of $a_p = \partial S / \partial B$ and M (the monodromy matrix) versus B for the principal periodic orbits of our model Hamiltonian. We have
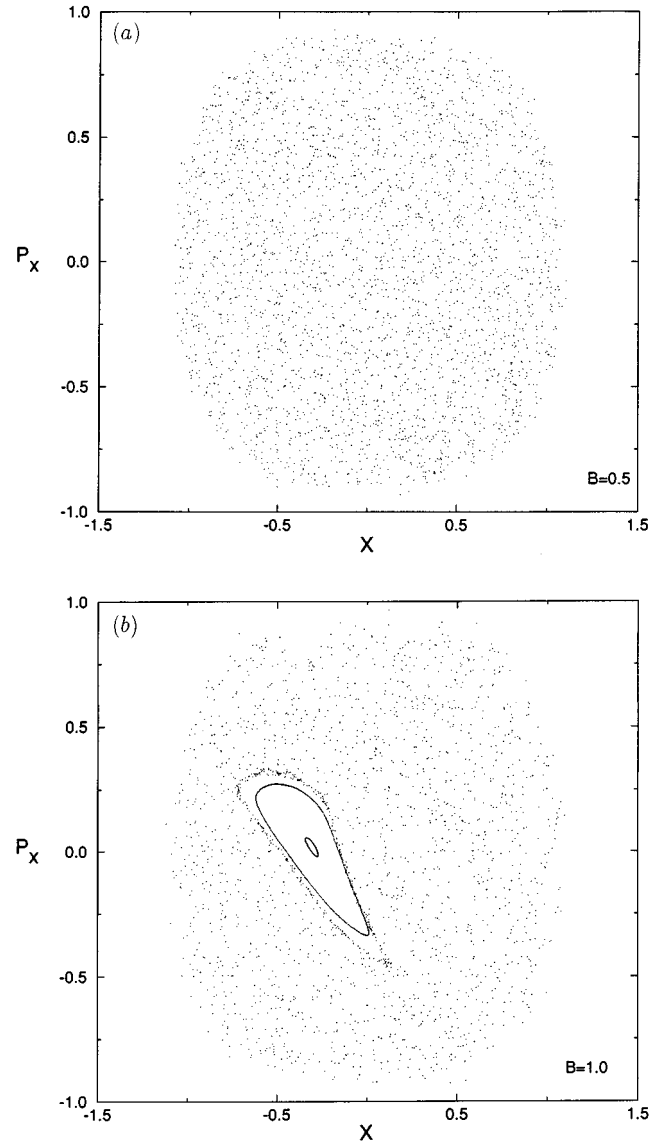

FIG. 5. $x - p_x$ Poincaré sections at energy $E = 0.403$ ($\hbar = 0.06$, $P = 50$) and magnetic fields: (a) $B = 0.5$; (b) $B = 1.0$.

computed these quantities and the results are shown in Fig. 6, for $E = 0.3146$ ($P = 30$) and $E = 0.403$ ($P = 50$). Here dashed (full) lines correspond to unstable (stable) families, and the circles to bifurcations with period doubling. The junction of full and dashed lines without symbols indicates isochronous bifurcations. The labels V, $V2$, $V3$, and $V4$ index the vertical family (the shortest orbit) and its bifurcations (doubling, tripling, and quadrupling) [8,13], which can easily be identified in Figs. 4(b), 4(d), and 4(e), respectively. The labels H, R, and L represent other families of periodic orbits. These families appear more clearly in $y - p_y$ sections, but they are not very relevant here because their periods are long.

The behavior of $V2$ for low fields is the most significant difference between Figs. 6(a) and 6(b): for $P = 30$ this family, initially stable, becomes unstable at $B \approx 0.4$ and stable again at $B \approx 0.47$. For $P = 50$, on the other hand, $V2$ is initially unstable and becomes stable at $B \approx 0.25$ (via an inverse pitchfork bifurcation) creating a new unstable family that, in
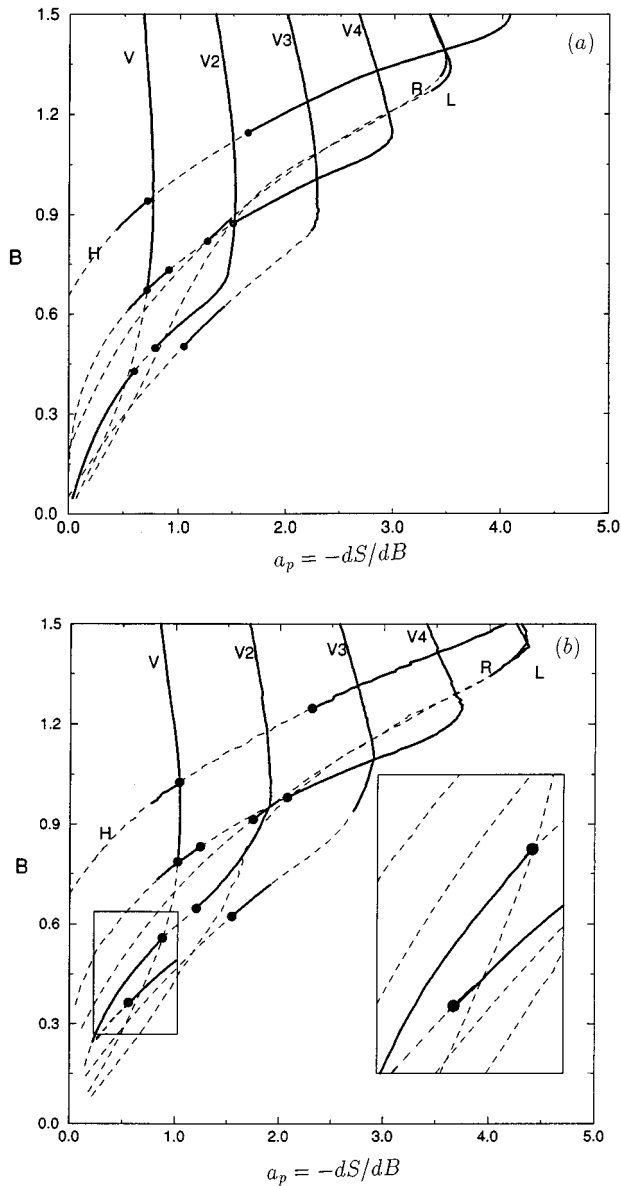
FIG. 6. Magnetic field B versus $a_p = dS/dB$ for the principal periodic orbits. (a) $E = 0.3146$ ($P = 30$, $\hbar = 0.06$) and (b) $E = 0.403$ ($P = 50$, $\hbar = 0.06$). The full (dashed) lines indicate stable-(unstable) regions and circles indicate period doubling bifurcations. The transitions from full to dashed lines without symbols indicate isochronous bifurcations.

its turn, become stable at $B \approx 0.34$ [see inset]. This bifurcated orbit turns out to be hard to follow numerically, and we show only part of it in the figure.

IV. NUMERICAL RESULTS FOR THE SUSCEPTIBILITY

We have computed the susceptibility per particle at zero temperature for the regular ($\hbar = 0.006$) and chaotic ($\hbar = 0.06$) cases. In Figs. 7 and 8 we compare these two cases for $P = 30$ and $P = 50$, respectively. As discussed in the preceding section, the regular susceptibility should be scaled by a factor of 10 in both figures because of our choices for $\hbar$. For $P = 30$ we see that, except for the sharp dips, the regular susceptibility increases approximately linearly with
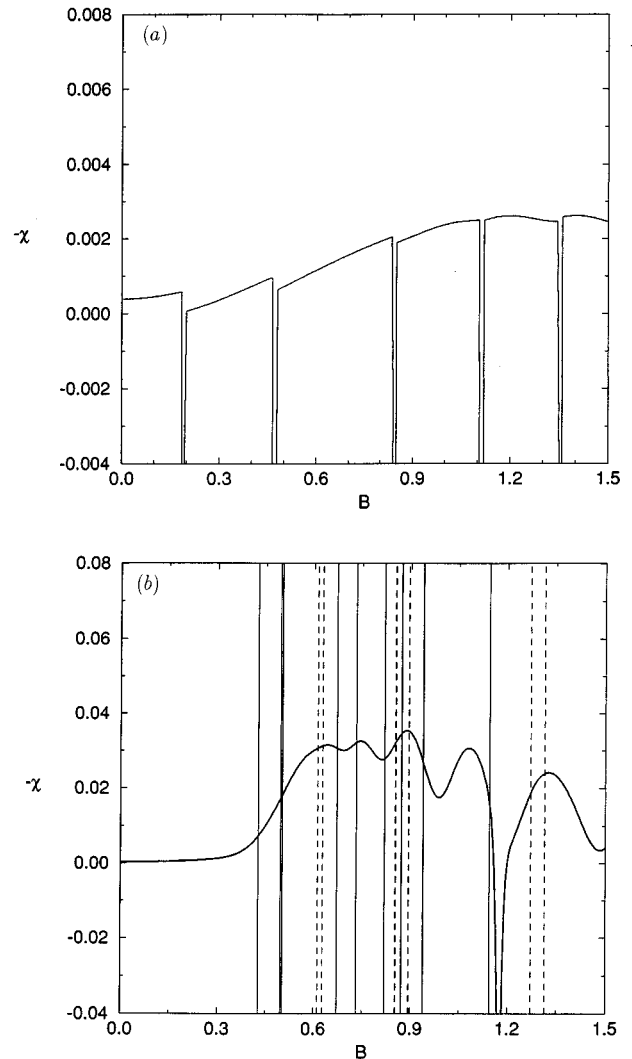

FIG. 7. $-\chi$ as a function of B for $P = 30$. (a) shows the result for the regular levels ($\hbar = 0.006$) and (b) shows the result for the chaotic levels ($\hbar = 0.06$). The full (dashed) vertical lines indicate values of B where period doubling(isochronous) bifurcations occur, according to Fig. 6(a).

the field, at least up to $B \approx 1.0$. This behavior can be understood in terms of the harmonic oscillator model analyzed by Németh [14], since our model is essentially quadratic at this energy.

The chaotic susceptibility, on the other hand, exhibits a very different behavior. For B up to 0.3 it has a negligible value, which is the Landau susceptibility, and a very small slope. For larger fields, however, we observe a clear transition to an oscillatory regime in which the magnitude of χ reaches values comparable to, or even higher than, those attained in the regular case. To understand these features semiclassically, we go back to Figs. 4 and 6(a). From the Poincaré sections we see that stable regions are seen only at $B = 0.6$ and therefore cannot be responsible for the sudden increase in $-\chi$ at $B \approx 0.4$. Figure 6(a), however, reveals that a series of bifurcations take place at that point. The values of B where the bifurcations occur are marked in Fig. 7(b) by vertical lines. We recall that at an isochronous bifurcation (dashed vertical line) the semiclassical amplitudes are diver-
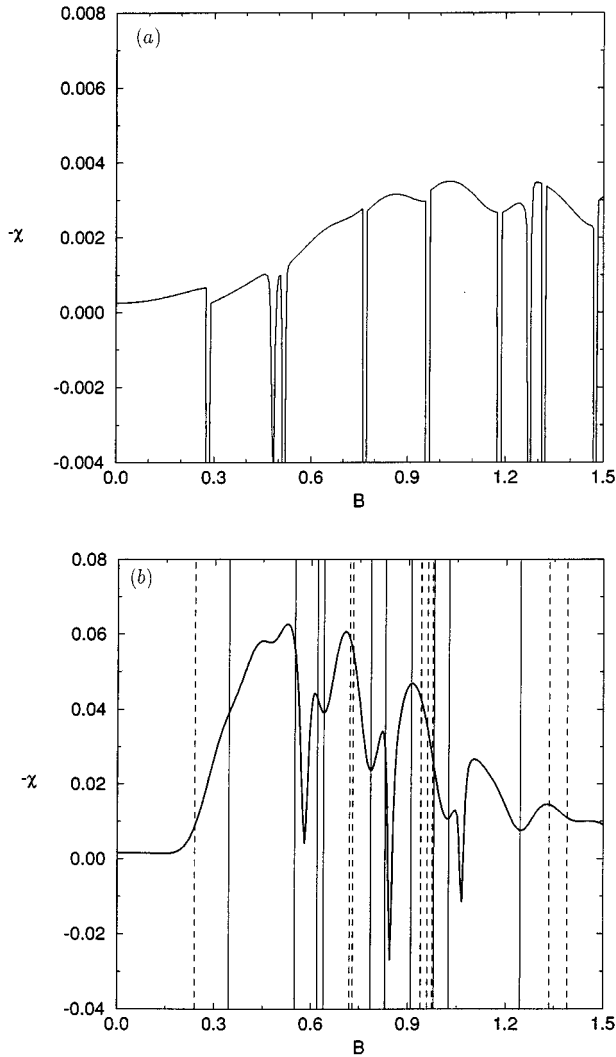
FIG. 9. $-\chi$ versus B for $P=30$. The thick (thin) line indicates χ_{chaot} ($\chi_{\text{reg}} \times 10$).

FIG. 8. $-\chi$ as a function of B for $P=50$. (a) shows the result for the regular levels ($\hbar=0.006$) and (b) shows the result for the chaotic levels ($\hbar=0.06$). The full (dashed) vertical lines indicate values of B where period doubling(isochronous) bifurcations occur, according to Fig. 6(b).

gent, whereas at a period-doubling bifurcation (continuous vertical line) it is the amplitude corresponding to the newly bifurcated orbit and the first repetition of the main orbit that diverge.

Figures 8(a) and 8(b), for $P=50$, show the same qualitative behavior, with the sudden increase in $-\chi$ at $B \approx 0.3$ related again to the bifurcations of periodic orbits, and not to the size of stability islands. It is interesting to note that the regularization process promoted by the magnetic field is triggered sooner for P=50 [Fig. 8(b)] than for P=30 [Fig. 7(b)], despite the fact that the periodic orbits have a larger instability exponent at $E=E_{50}(B=0)$ than at $E=E_{30}(B=0)$.

The comparison between χ_{reg} and χ_{chaot} for low fields is more explicit in Fig. 9, where we plot $\chi_{\text{reg}} \times 10$ and χ_{chaot} for $B \leq 0.1$ and $P=30$. In this case, the regular Poincaré section, Fig. 1(a), does not show any visible chaos while the chaotic section, Fig. 4(a), is entirely chaotic. So, we can see that for low fields $\chi_{\text{reg}} \gg \chi_{\text{chaot}}$ as expected [4].

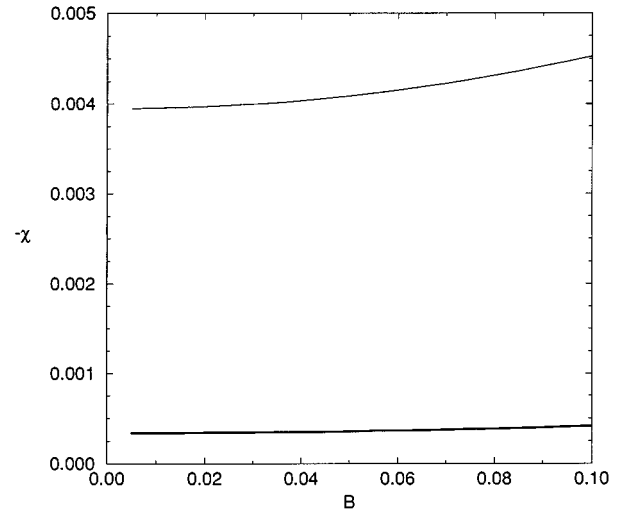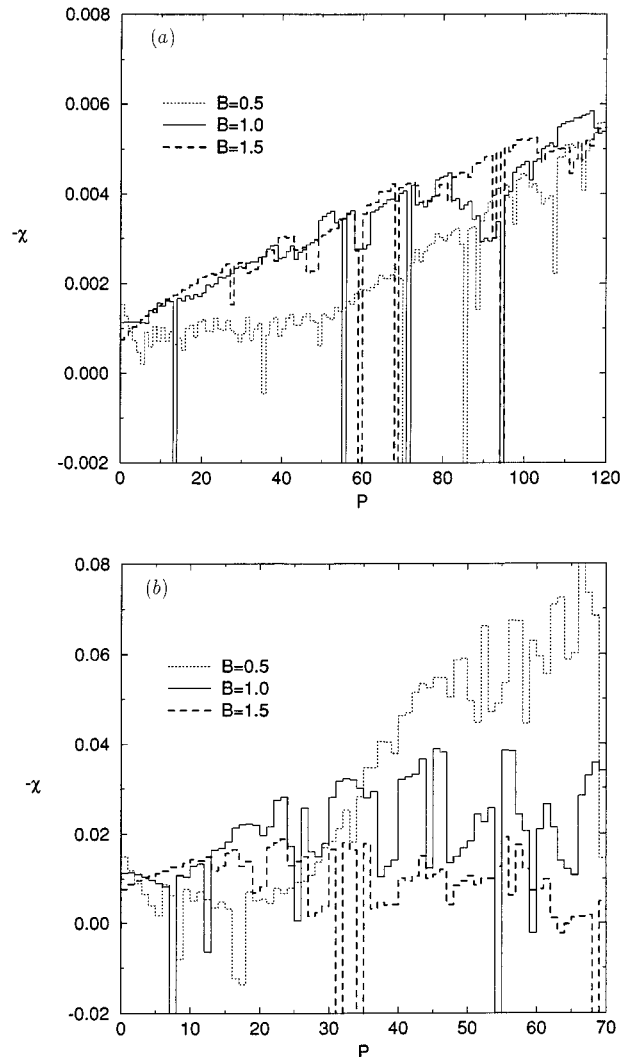We now investigate the robustness of our results in terms

FIG. 10. $-\chi$ as a function of P: (a) regular levels and (b) chaotic levels.
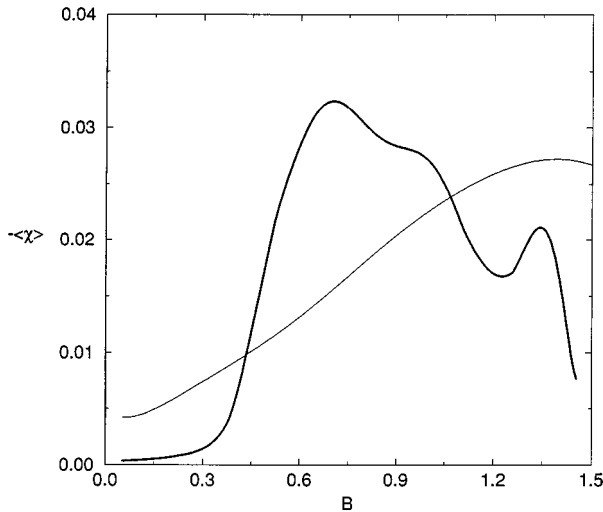
FIG. 11. $-\langle\chi\rangle$ as a function of B for $\overline{P}=30$ and $\Delta=5$. The thick (thin) line indicates $\langle\chi_{\text{chaot}}\rangle$ ($\langle\chi_{\text{reg}}\rangle\times10$).

of ensemble averages. For simplicity we consider a Gaussian average defined by

$$\langle\chi\rangle=\frac{1}{2\Delta\sqrt{\pi}}\sum_{P=0}^{\infty}\chi(B,P)\exp[-(P-\overline{P})^2/4\Delta^2]. \quad (19)$$

Figure 10 shows $-\chi$ as a function of P for some values of the magnetic field for both the regular [Fig. 10(a)] and chaotic [Fig. 10(b)] cases. Here the differences between the two are also visible. The regular case is very simple and, for a fixed P, χ_{reg} increases with the field. In contrast, we see that the chaotic case exhibits the opposite behavior for large P and a complex oscillation for P between 20 and 40. Figure 11 shows $\langle\chi\rangle$ as a function of B for $\overline{P}=30$ and $\Delta=5$. At intermediate field values the average chaotic susceptibility is greatly enhanced in comparison with the regular χ, further emphasizing the effect of bifurcations.

Finally, we compare the canonical versus grand-canonical averages for the chaotic case. As discussed by Altshuler, Gefen, and Imry [6] we expect a vanishingly small susceptibility if the average in Eq. (19) is performed in the grand-canonical ensemble. Figure 12 displays these averages as a function of $\overline{P}$ for $B=0.8$ and two values of the dispersion parameter Δ, and clearly exhibits good agreement with the theory.

V. CONCLUSIONS

We have studied the magnetic susceptibility of a mesoscopic ensemble of noninteracting electrons at zero temperature confined by a smooth potential. We found that χ depends strongly on the underlying classical dynamics. If the magnetic field is weak enough, such that we can neglect its effect on the classical orbits, the susceptibility will be larger for a regular than for a chaotic confining potential, in agreement with previous results [4]. However, when the field is increased further, the nature of the classical dynamics inevitably changes. For initially chaotic potentials, the magnetic field will regularize the phase space by turning unstable pe-
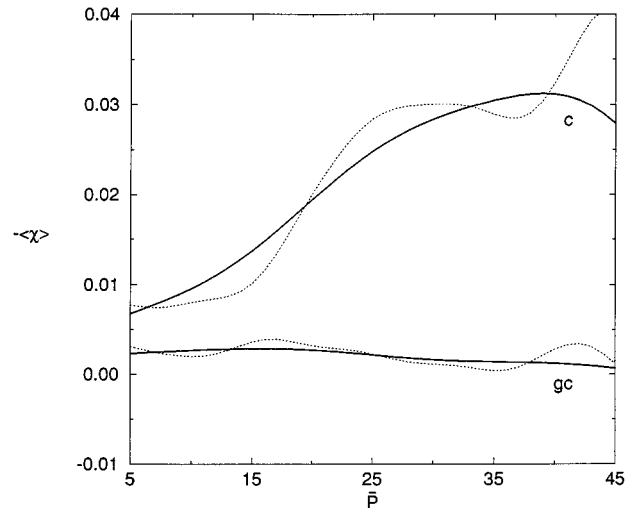

FIG. 12. $-\langle\chi\rangle$ versus $\overline{P}$ for the canonical(c) and grand-canonical(gc) ensembles at $B=0.8$ (chaotic case only). The thick-(dotted) lines indicate $\Delta=5(2)$ in Eq. (19).

riodic orbits into stable ones, or in other words, by inducing bifurcations. We have shown here that these bifurcations contribute significantly to χ, even when the phase space is still mostly chaotic. If the potential is initially regular, the field will first introduce some chaos (except, of course, for the case of radially symmetric potentials) and then, for higher fields, regularize it again.

From the classical point of view, the magnetic field B becomes important when the cyclotron radius $R=\sqrt{2E}/B$ ($e=m=c=1$) is comparable with the typical length scale of the system, L. In fact, the effects of B can be felt quite strongly even when $R\approx10L$ for geometries like the square billiard [15]. The quantum mechanical length scale, or magnetic length, on the other hand, is given by $b=\sqrt{\hbar/B}$. Therefore, at the Fermi energy $\mu=2\pi\hbar^2\rho$, the two scales are related by

$$R=b^2\sqrt{4\pi\rho},$$

where ρ is the electron density. In the experimental setup of Lévy et al. [1], when $b\approx L$ implies $R/b\approx10-100$, justifying the approximation in which the bending of the classical trajectories can be neglected. Therefore, we expect the susceptibility to go to zero before any classical chaos (or any important bifurcations) sets in. In order to observe the effects described in this paper a similar experimental setting would require either a lower density of electrons (by a factor $10-100$) or larger squares (by a factor $5-10$).

[1] L.P. Lévy, D.H. Reich, L. Pfeiffer, and K. West, Physica B **189**, 204 (1993).

[2] S.D. Prado, M.A.M. de Aguiar, J.P Keating, and R. Egydio de Carvalho, J. Phys. A **27**, 6091 (1994).

[3] O. Agam, J. Phys. (France) I **4**, 697 (1994).

[4] F. von Oppen, Phys. Rev. **B 50** 17 151 (1994).

[5] D. Ullmo, K. Richter, and R. Jalabert, Phys. Rev. Lett. **74**, 383 (1995).

[6] B. L. Altshuler, Y. Gefen, and Y. Imry, Phy. Rev. Lett. **66**, 88 (1991).

[7] M. C. Gutzwiller, J. Math. Phys. **12**, 243 (1971).

[8] S. D. Prado and M. A. M. de Aguiar, Ann. Phys. (N.Y.) **231**, 290 (1994).

[9] M. A. M. de Aguiar, C. P. Malta, M. Baranger, and K. T. R. Davies, Ann. Phys. (N.Y.) **180**, 167 (1987); M. A. M. de Aguiar and C. P. Malta, Physica D **30**, 413 (1988).

[10] A. M. Ozorio de Almeida and J. H. Hannay, J. Phys. A **20**, 5873 (1987).

[11] P. J. Richens, J. Phys A **15**, 2101 (1982).

[12] D. Provost and M. Baranger, Phys. Rev. Lett. **71**, 662 (1993).

[13] M. Baranger and K.T.R. Davies, Ann. Phys. (N.Y.) **177**, 330 (1987).

[14] R. Németh, Z. Phys. A **81**, 89 (1990).

[15] N. Berglund and H. Kunz, J. Stat. Phys. **83**, 81 (1996); M. A. M. de Aguiar, Phys. Rev. E **53**, 4555 (1996).